Atmos. Chem. Phys., 12, 2713–2723, 2012
www.atmos-chem-phys.net/12/2713/2012/
doi:10.5194/acp-12-2713-2012

Atmospheric Chemistry and Physics

Analysis of $\Delta O_2/\Delta CO_2$ ratios for the pollution events observed at Hateruma Island, Japan

C. Minejima[1,*], M. Kubo[2], Y. Tohjima[1], H. Yamagishi[1], Y. Koyama[1], S. Maksyutov[1], K. Kita[3], and H. Mukai[1]

[1]National Institute for Environmental Studies, Tsukuba 305–8506, Japan
[2]Graduate School of Science and Engineering, Ibaraki University, Mito, Ibaraki 310-8512, Japan
[3]Faculty of Science, Ibaraki University, Mito, Ibaraki 310–8512, Japan
[*]now at: Department of Chemical Engineering, Tokyo University of Agriculture and technology, 184–8588, Japan

Correspondence to: C. Minejima (minejima@cc.tuat.ac.jp)

Received: 11 May 2011 – Published in Atmos. Chem. Phys. Discuss.: 23 May 2011
Revised: 2 February 2012 – Accepted: 6 February 2012 – Published: 14 March 2012

Abstract. Pollution events extracted from the in situ observations of atmospheric CO_2 and O_2 mixing ratios at Hateruma Island (HAT, 24° N, 124° E) during the period from October 2006 and December 2008 are examined. The air mass origins for the pollution events are categorized by using back trajectory analysis, and the oxidative ratios ($OR = -O_2{:}CO_2$ molar exchange ratio) for selected pollution events are calculated. We find that there is a significant difference in the average oxidative ratios between events from China ($OR = 1.14 \pm 0.12$, $n = 25$) and Japan/Korea ($OR = 1.37 \pm 0.15$, $n = 16$). These values are in a good agreement with the national average oxidative ratios for the emissions from fossil fuel burning and cement production (FFBC) in China ($OR_{FFBC} = 1.11 \pm 0.03$) and Korea/Japan ($OR_{FFBC} = 1.36 \pm 0.02$). Compared with the observation, simulations of the atmospheric O_2 and CO_2 mixing ratios using Lagrangian particle dispersion models do a good job in reconstructing the average oxidative ratio of the pollution events originating in China but tend to underestimate for events originating in Japan/Korea. A sensitivity test suggests that the simulated atmospheric oxidative ratios at HAT are especially sensitive to changes in Chinese fuel mix.

1 Introduction

There is a tight negative stoichiometric coupling between oxygen (O_2) flux and carbon dioxide (CO_2) flux of land biotic respiration and photosynthesis processes and burning processes of fossil fuels and biomass. In order to express the quantitative coupling between O_2 and CO_2, the oxidative ratio is defined as the $-O_2{:}CO_2$ molar exchange ratios: $OR = -\Delta O_2[\text{mol}]/\Delta CO_2[\text{mol}]$. The oxidative ratios are different for the land biotic and burning processes because the ratio is basically dependent on the elemental compositions of related organic and inorganic matters. Keeling (1988) estimated the oxidative ratios for coal, liquid fuel, and natural gas burning to be 1.17 ± 0.03, 1.44 ± 0.03 and 1.95 ± 0.04, respectively. The estimated global average oxidative ratio for land biotic processes is 1.10 ± 0.05 (Severinghaus, 1995). On the other hand, an analogous stoichiometric coupling between O_2 and CO_2 fluxes for air-sea gas exchange processes does not exist because oceanic CO_2 flux is significantly suppressed by a chemical equilibrium between dissolved CO_2, bicarbonate and carbonate ions.

The O_2 and CO_2 fluxes from land biotic and burning processes should cause the correlative changes in the atmospheric mixing ratios of O_2 and CO_2 downwind of the source region. Recent improvements in O_2 measurement technique have enabled the detection of high-frequency changes in atmospheric O_2 mixing ratios simultaneously with that of CO_2 (Manning et al., 1999; Stephens et al., 2003; Yamagishi et al., 2008). Accordingly, the oxidative ratios calculated as $-\Delta O_2/\Delta CO_2$ regression slopes for such short-term O_2 and CO_2 variations have recently been used to constrain the contributions from individual sources. For example, Stephens et al. (2003) conducted continuous in situ measurements of O_2 and CO_2 on research cruises in the equatorial Pacific and Southern Oceans and concluded that some short-term variations with $OR = \sim 1.4$ were caused by the combustion of liquid fossil fuels. Examining the short-term atmospheric O_2 and CO_2 variations over a forest canopy at

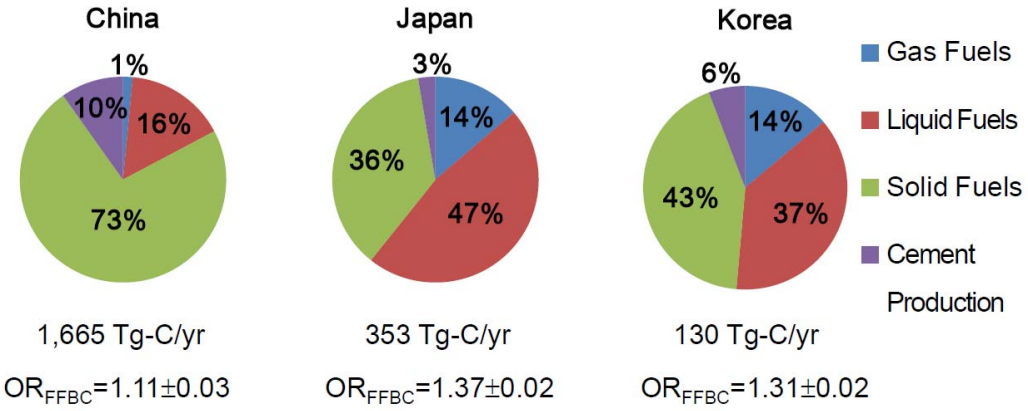

Fig. 1. Compositions of fuel mix used in China, Japan and Korea in 2006 (Boden et al., 2010, Keeling, 1988).

the WLEF tall-tower research site in northern Wisconsin, USA, Stephens et al. (2007) found that the ORs during winter range from 1.41 to 1.53, which is close to the average OR of 1.45 derived from the US fuel mix estimate in 2000. In addition, Sirignano et al. (2010) and van der Laan-Luijkx et al. (2010) investigated the influence of the Dutch fossil fuel mix ($OR = 1.69 \pm 0.06$), which has a proportionally high natural gas component, on the atmospheric observation at Lutjewad and computed the observable OR of 1.49 with significant seasonality: lower in summer and higher in winter. To investigate the spatiotemporal variations in the ORs based on the atmospheric O_2 and CO_2 observations, Steinbach et al. (2011) developed a global data set of CO_2 emission and O_2 uptake associated with the fossil fuel burning.

The National Institute for Environmental Studies (NIES) has been measuring atmospheric O_2 and CO_2 by flask sampling at Hateruma Island (HAT, 24° N, 124° E) since July 1997 at a frequency of several flasks per month (Tohjima et al., 2003, 2008). To capture more frequent O_2 variations, we started in situ O_2 measurements at HAT from October 2006. Since the prevailing wind direction in the winter time is northwest due to the East Asian monsoon, the observations at HAT often show pollution events influenced by emissions from East Asian countries from late fall to early spring each year (Tohjima et al., 2002, 2010). These pollution events observed at HAT have been used to estimate the national emissions of HFCs and HCFCs from China, Korea, and Japan (Yokouchi et al., 2006; Shirai et al., 2010). Therefore, this setting of HAT gives us confidence in the unique location of the HAT observational site for analyzing the relationship between O_2 and CO_2 variations in the pollution events originating from East Asian source regions. In fact, there is significant difference in the national average oxidative ratios for the emissions from fossil fuel burning and cement production (FFBC) coming from China ($OR_{FFBC} = 1.11 \pm 0.03$), Japan ($OR_{FFBC} = 1.37 \pm 0.02$) and Korea ($OR_{FFBC} = 1.31 \pm 0.02$). These oxidative ratios are calculated using the fuel mix of the respective countries taken from the CDIAC inventories for the year 2006 (Boden et al., 2010) and the oxidative ratios for the 3 main fuel types (Keeling, 1988) and the cement manufacturing ($OR_{cement} = 0$). It should be noted that the higher percentage of the CO_2 emissions from coal and cement production for China results in a significantly lower oxidative ratio in comparison with Japan and Korea (Fig. 1).

In this study, we investigated the oxidative ratios of pollution events observed at HAT. Source regions of the individual pollution events were identified via back trajectory analysis, and the observed oxidative ratios were compared with the oxidative ratios calculated from the reported compositions of the fossil fuel types at their trajectory origins. Furthermore, in order to examine the relative impact of fossil fuel types used and the variations in the regional emission to the observed O_2 and CO_2 changes at HAT, we employed an atmospheric transport model FLEXPART that uses the Lagrangian particle dispersion scheme (Stohl et al., 1998). Based on the comparison between the observation and the model result, we examined the possibility that the observed oxidative ratios can be used as an independent mean to verify the inventories of CO_2 emissions based on the national fossil fuel mixes.

2 Observation data and analytical methods

2.1 Observation at HAT

HAT is a small elliptical (longer in the east-west direction) island with an area of 12.7 km^2 and a population of 600, and is located at the southern edge of Japanese archipelago. The monitoring station is situated on the eastern edge of the island, and the prevailing wind direction at the station is northerly in winter and southerly in summer. Local emissions from the island were determined to be not a significant influence on the observations at HAT.

Sample air is drawn from an inlet placed on the tower at the height of 36.5 m a.g.l. (46.5 m a.s.l.) at a flow rate of about 8 l min^{-1} by using a diaphragm pump. Then, the sample air is introduced into a 2-l spherical Pyrex-glass flask at a pressure of 0.06 MPa (relative to ambient), which is kept by using a back pressure regulator. The air sample is collected from the center of the spherical flask using a 1/16 inch OD stainless steel tubing at a continuous flow rate of 8 ml min^{-1}. This air sampling system considerably reduces the fractionation effects on the O_2/N_2 ratio (Yamagishi et al., 2008), which could occur at the air inlet (Blaine et al., 2006) and the tee-junction (Stephens et al., 2007). The collected air sample is dried by passing through cold traps, and then introduced into the O_2/N_2 measurement system that includes a gas chromatograph equipped with a thermal conductivity detector (GC/TCD). Details of the sampling, analyzing and data processing methods are described elsewhere (Tohjima, 2000; Yamagishi et al., 2008). The CO_2 mixing ratios are continuously measured by a nondispersive infrared analyzer (NDIR) (Mukai et al., 2001).

Changes in O_2 mixing ratios are expressed as a relative deviation of the O_2/N_2 ratio from an arbitrary reference according to

$$\delta(O_2/N_2) = [(O_2/N_2)_{sample}/(O_2/N_2)_{reference} - 1] \times 10^6. \quad (1)$$

Following Keeling and Shertz (1992), we use the units of "per meg" to express the $\delta(O_2/N_2)$ value. A value of 4.8 per meg is equivalent to 1 µmol mol^{-1} (ppm) in a trace gas abundance. Here, the $\delta(O_2/N_2)$ values are determined against our original reference scale (Tohjima et al., 2008). The O_2/N_2 ratio was measured every 10 min and the standard deviation of the O_2/N_2 ratio measurement is estimated to be $\pm$ 14 per meg ($\sim$3 ppm), thus has a standard error of $\pm$ 6 per meg ($\sim$1.2 ppm) for an one-hour average. The CO_2 values are reported on the NIES gravimetric standard scales (NIES-09) based on the CO_2-in-air standard gases prepared by gravimetric one-step dilution method (Machida et al., 2011). The CO_2 analytical precision is about 0.1 ppm.

In this study, we analyze the hourly O_2 and CO_2 mixing ratios observed during the period from October 2006 to December 2008 (Fig. 2). The observed CO_2 clearly shows secular increasing trend and seasonal cycle with an increase in the fall and winter and decrease in the spring and summer, while the observed O_2 shows the opposite trend and seasonal cycle. In addition, CO_2 and O_2 show short-term variations on synoptic time scales associated with pollution events, especially in late fall to early spring. In the following sections, we will focus on the analysis of this short-term component of the atmospheric signal.

2.2 Correlation analysis of pollution events

In order to extract the short-term variation components of CO_2 and O_2, we first obtain smooth-curve fits to the data following the methods of Thoning et al. (1989) with a cut-off

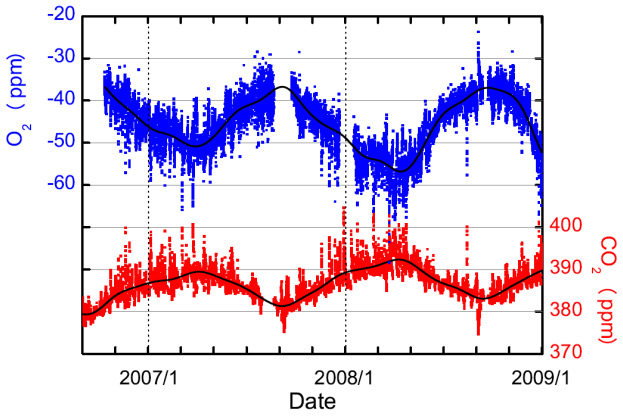

Fig. 2. Time series of atmospheric (blue) O_2 and (red) CO_2 mixing ratios observed at HAT for whole period of this study. Each dot represents hourly average. The smooth curve fits to the data are shown as solid lines.

frequency of 4.6 cycles yr^{-1} (see Fig. 2), and then subtract the smooth-curve fits from the original time series. Hereafter, the extracted short-term variations are denoted by the Δ notation as ΔCO_2 and ΔO_2.

As an example, hourly ΔCO_2 and ΔO_2 measurements over a one-month period (7 November to 22 December 2007) are shown in Fig. 3a and b, respectively. From these short-term variations, we identified pollution events as follows: First, we found largely varying ΔCO_2 events where the difference between the maximum and minimum is larger than 4.1 ppm (twice the standard deviation of whole ΔCO_2) and the duration ranged from 12-h to 3-days. It should be noted that the start and end times of each pollution event peak are determined manually; however, the following correlation analyses are not sensitive to the choice of the start and end time. Then the correlation coefficient (r) between ΔO_2 and ΔCO_2 variations and the linear regression slope ($\Delta O_2/\Delta CO_2$) are computed for each event. From the linear regression slope, we obtain the oxidative ratio for the pollution event as OR = $-\Delta O_2/\Delta CO_2$. For the following analysis, we discarded events with $|r| < 0.8$. Adopting this criterion, we eliminated about 25 % of the pollution events and in total, we analyzed 67 pollution events in the following analysis. For example, we identified three pollution events during the 1-month period as shown in Fig. 3.

We categorize the origins of the pollution events into 3 regions: China, Japan/Korea and "other origins" using a kinematic 5-day back trajectory calculated by the METeorological data Explorer (METEX, http://db.cger.nies.go.jp/metex/) (Zeng et al., 2003). Altitude of the starting point for the calculation is set at 40 m a.g.l., which is close to the altitude of the sample inlet. Arrival time of each air mass corresponds to the time when the highest CO_2 mixing ratio in each event is observed.

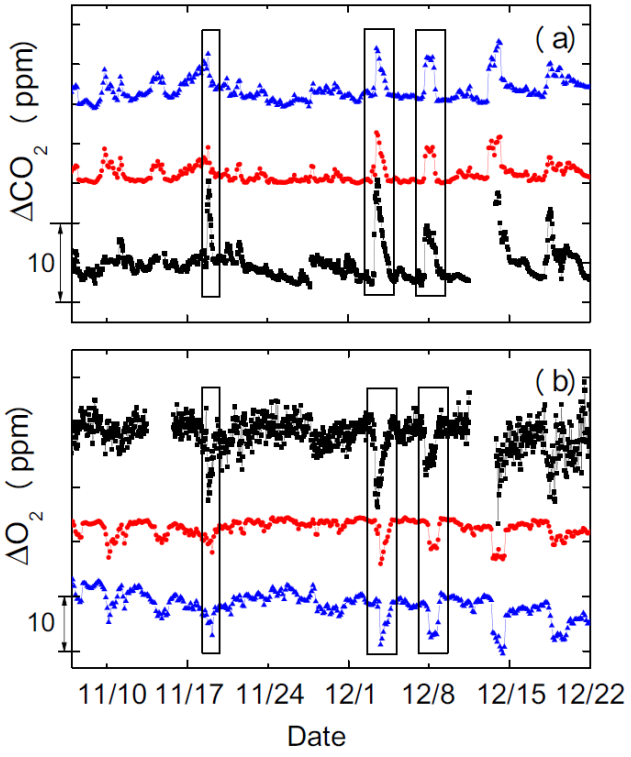

Fig. 3. Short-term variations in **(a)** ΔCO_2 (ppm) and **(b)** ΔO_2 (ppm) for the 1-month period (mid November to mid December, 2007). Each dot represents hourly average. Black squares are observations, red circles are model simulation by FLEXPART and blue triangles are model simulation by the coupled model. Pollution events analyzed in this study are enclosed with the black rectangulars.

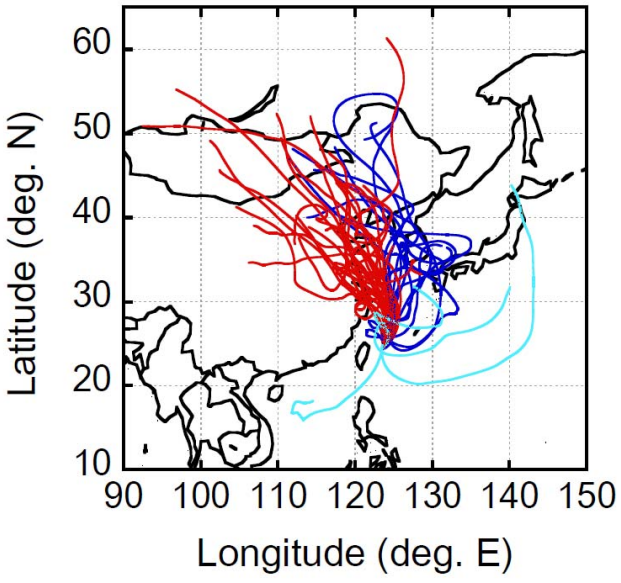

Fig. 4. Five-day back trajectories observed at HAT. The air mass origins are categorized into three regions: China (Red), Japan/Korea (Blue) and "other" (Cyan). All events from China and Japan/Korea are depicted and four events from "other" are drawn as examples.

In the back trajectory calculations, the National Center for Environmental Prediction (NCEP) reanalysis data with a time resolution of 6 h, latitude/longitude grid of 2.5 degree and 17 pressure levels are used (Kistler et al., 2001). The first country to intersect the back trajectory is assigned as the origin of the air mass. Among the 67 pollution events, 25 and 16 events are assigned to China and Japan/Korea origins, respectively. Fig. 4 shows all resulting trajectories assigned to China and Japan/Korea as their origins as well as four example events assigned to "other origins".

2.3 Model simulation

2.3.1 Lagrangian Particle Dispersion Model (LPDM), FLEXPART

In order to investigate the influence of regional fluxes and the contributions of individual flux categories such as FFBC fluxes, land biotic fluxes, and oceanic exchanges to the pollution events, a Lagrangian particle dispersion model, FLEXPART v3.2 (Stohl et al., 1998), is used in this study. FLEXPART calculates the trajectories of multiple tracer particles using mean winds interpolated from the meteorological fields and random motions representing turbulences. Three-hourly meteorology data from Global Forecast System (GFS) provided by the National Center for Environmental Prediction (NCEP) are used as the meteorological fields, which have a spatial resolution of $1^\circ \times 1^\circ$. In each simulation, 10 000 particles are released from a receptor position (the inlet of the tower at HAT in this study) and transported eight days backward in time. The time step of the calculation is 900 s and each transported particle absorbs the CO_2 and O_2 fluxes ($kg\,m^{-2}\,day^{-1}$) of its location once a day when it is located under the altitude of 1000 m. Changing the criterion altitude where the particles absorb the fluxes from 300 m to 2000 m, we found no significant difference in resultant CO_2 mixing ratios. At last, CO_2 and O_2 fluxes each particle absorbed are summed and mixing ratios were calculated using the method developed by Seibert and Frank (2004). The CO_2 and O_2 mixing ratio changes calculated this way include the influence of fluxes and meteorology for the previous eight days, which gives enough time for particles to spread over East Asia.

The CO_2 flux from FFBC was calculated using the fossil98 flux data that was employed in the TransCom model simulation (Law et al., 2008). The fossil98 flux dataset was based on the EDGARV32 CO_2 emission map with the spatial resolution of $1^\circ \times 1^\circ$ for the year 1990 (Olivier and Berdowski, 2001), which was then scaled to the emission level of 1998 using the CDIAC totals. We used the individual national total emissions for the years 2006, 2007, and 2008 from the

Table 1. Summary of the average OR for the individual air mass origins and OR_{FFBC} for the corresponding countries.

	OR[a]			OR^{b}_{FFBC}
Air mass origin	Observation	FLEXPART	coupled model	CDIAC
China	1.14 ± 0.12 (25)	1.08 ± 0.10 (14)	1.07 ± 0.11 (14)	1.11 ± 0.03
Japan/Korea	1.37 ± 0.15 (16)	1.09 ± 0.14 (13)	1.19 ± 0.15 (13)	1.36 ± 0.02
Other	1.20 ± 0.20 (26)	1.15 ± 0.16 (14)	1.18 ± 0.18 (14)	$(1.27 \pm 0.10)^{c}$

[a] Uncertainties correspond to the standard deviations. Numbers in the parentheses represent numbers of events.

[b] Uncertainties correspond to propagated errors of the ORs for individual fuel type and national fossil carbon emissions. The ORs for coal, liquid fuel, natural gas burning and gas flaring are 1.17 ± 0.03, 1.44 ± 0.03, 1.95 ± 0.04, and 1.98 ± 0.07, respectively (Keeling, 1988). For the uncertainties associated with the national fossil carbon emissions, ± 15 % is used for China (Gregg et al., 2008) and ± 6 % is used for the other countries (Marland and Rotty, 1984).

[c] Average value of OR_{FFBC} for China, Japan, Korea, Taiwan, and Philippines. The uncertainty corresponds to the standard deviation (1σ).

CDIAC database to scale the fossil98 CO_2 emission map for the top 20 CO_2 emitting countries. The emissions from rest of the world were scaled to match the global total CO_2 emission of the year. Note that the FFBC CO_2 fluxes for the year 2008 were estimated by extrapolating the rate of increase from 2006 to 2007 for the top 20 countries. The biospheric CO_2 uses optimized CASA flux (Nakatsuka and Maksyutov, 2009) and oceanic component is air-sea CO_2 flux from Takahashi et al. (2002). The biospheric and oceanic fluxes are available monthly and they are converted into daily fluxes through linear interpolation.

The O_2 fluxes from FFBC were prepared by multiplying the CO_2 flux from FFBC by the oxidative ratios calculated from the corresponding fuel compositions. The national FFBC oxidative ratios of 1.11, 1.37 (1.38 in 2007 and 2008), and 1.31 for China, Japan, and Korea, respectively, are used to calculate the O_2 fluxes for the 3 years of 2006, 2007, and 2008. For the remaining countries, a single oxidative ratio of 1.45 based on the average fuel compositions of these remaining countries is used for the O_2 flux map for the 3 years. Similarly, the O_2 fluxes from the terrestrial biosphere (TB) are prepared as a product of the optimized CASA flux and the land biotic oxidative ratio of 1.1. For O_2 flux from ocean, we use the monthly mean climatological oceanic fluxes of Garcia and Keeling (2001).

2.3.2 The global coupled Eulerian-Lagrangian transport model (the coupled model)

The atmospheric CO_2 and O_2 changes predicted by FLEXPART only reflect the regional fluxes within the range of locations of dispersed particles for up to eight days in this study. In order to include larger scale background influence, we also use a global coupled Eulerian-Lagrangian transport model (coupled model) developed by Koyama et al. (2011). It is comprised of a global Eulerian transport model, the NIES-TM (Maksyutov et al., 2008), and a regional LPDM, FLEXPART. The NIES-TM component gives the initial mixing ratio of the air mass eight days in the past, and FLEXPART gives the eight days plume transport for 10 000 particles. The CO_2 mixing ratios simulated by NIES-TM at the location of each particle at eight days back is averaged to predict the influence of the background CO_2 mixing ratio. The same flux set that was used for FLEXPART was used for the coupled model. NIES-TM is driven by JCDAS-25 and is run with a horizontal resolution of $2.5^\circ \times 2.5^\circ$, with 15 sigma levels. JCDAS-25 has a time resolution of 12-h and a spatial resolution of $2.5^\circ \times 2.5^\circ$.

3 Results

3.1 Observed oxidative ratios

The oxidative ratios for the observed pollution events categorized as the China and Japan/Korea origins are shown in Fig. 5a, plotted against time of the year. There is no pollution event between May and September in the figure because all the events during the period are assigned to "other origins". The oxidative ratios for all the events from both regions show large variability with a range from 1.0 to 1.7. The oxidative ratios for events with origins in China, however, tend to be lower (ranging from 1.0–1.4) than those with origins from Japan/Korea (1.1–1.7). The average oxidative ratios are 1.14 ± 0.12 for China and 1.37 ± 0.15 for Japan/Korea, respectively (uncertainties given here are 1σ standard deviations). The Welch's t-test reveals that the average oxidative ratios between China and Japan/Korea events differ with more than a 99.9 % confidence level. These averages of the observed oxidative ratios show excellent agreements with the FFBC oxidative ratios for China ($OR_{FFBC} = 1.11 \pm 0.03$) and Japan/Korea ($OR_{FFBC} = 1.34 \pm 0.02$), which are calculated from 2006 national fossil carbon inventories provided by CDIAC database. These values are summarized in Table 1 and are plotted in Fig. 6.

These results suggest that the observed air masses arriving at Hateruma predominantly reflect the characteristics of CO_2 emission and O_2 consumption from fossil fuel burning at their source regions.

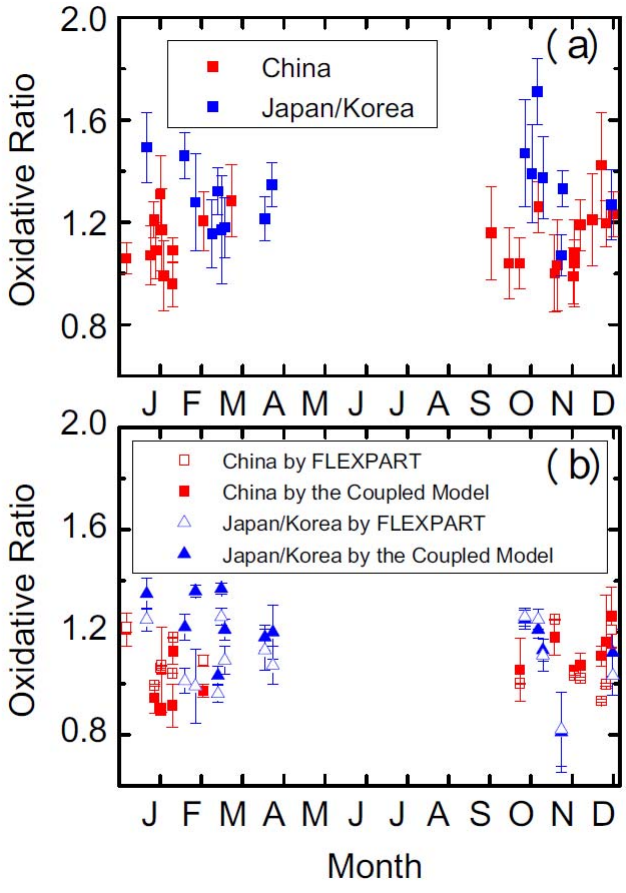

Fig. 5. Calculated oxidative ratios from -$\Delta O_2/\Delta CO_2$ regression slopes of each pollution event for **(a)** observation and **(b)** model simulations. Red and blue symbols are for events from China and Japan/Korea, respectively. In **(b)**, open symbols are based on FLEXPART and closed symbols are based on the coupled model.

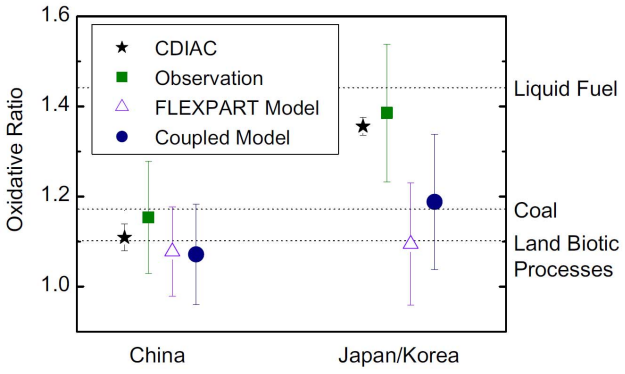

Fig. 6. Oxidative ratios for the fossil carbon emissions from China and Japan/Korea, and average oxidative ratios for the China and Japan/Korea pollution events based on the observations and model simulations using FLEXPART and the coupled model. The national emission inventories of the fossil carbon from the CDIAC database are used to calculate the oxidative ratios for FFBC emissions. The vertical bar of CDIAC is the same as Table 1. The standard deviations are shown as vertical bars for observation, FLEXPART Model and Coupled Model. Dotted black lines show estimated oxidative ratios for land biotic processes (Severinghaus, 1995), coal, and liquid fuel burning (Keeling, 1998).

3.2 Simulated oxidative ratios

Figure 3 also shows the time series of the hourly ΔCO_2 and ΔO_2 data simulated by FLEXPART and the coupled model. The model results generally well reproduce the observed pollution events. However, precise comparisons reveal that there are often differences in the phase and size between the simulated and observed CO_2 and O_2 short-term variations associated with the pollution events. Therefore, the simulated pollution events whose phases are off by more than 10 h and whose sizes are less than 1.4 ppm (twice the standard deviation of whole modeled ΔCO_2) are discarded in the following analysis. Using these criteria, we obtain 27 pollution events (14 China events and 13 Japan/Korea events) by the FLEXPART and the coupled model simulations. Note that all the correlation coefficients for the simulated CO_2 and O_2 variations of the selected 27 pollution events are larger than 0.8.

Figure 5b shows the oxidative ratios of the 27 pollution events calculated by FLEXPART and the coupled model. In general, the oxidative ratios of FLEXPART and the coupled models agree well with each other although the Japan/Korea events in February and March show slightly different oxidative ratios between the two models.

Figure 7 shows a scatter plot of the oxidative ratios simulated by FLEXPART versus the observed ratios. The model-simulated oxidative ratios do not necessarily reconstruct the individual observed ratios. When all events in Fig. 7 are taken as a group, a high correlation is not seen. However, upon examining the relationships for the China events and Japan/Korea events separately, we find significant correlation for the Japan/Korea events with a correlation coefficient (r) of 0.79 and a regression slope of 0.71. On the other hand, both the observed and simulated oxidative ratios of China events have small variations and are clustered around 1.1.

The averages of the oxidative ratios for the model predictions together with those of observations are also summarized in Table 1 and are plotted in Fig. 6. The averages of the observed and simulated oxidative ratios for the China events agree well with a 95 % confidence level (Welch's t-test). On the other hand, for the Japan/Korea events the simulated oxidative ratios are significantly lower than those of the observation with the same confidence level. Some of the average oxidative ratios from the model predictions are slightly smaller than the land biotic oxidative ratio of 1.1. During this time of the year, the mid-latitude regions of the western North Pacific Ocean act as a sink for atmospheric CO_2 and O_2, with the O_2 fluxes exceeding the CO_2 fluxes. As

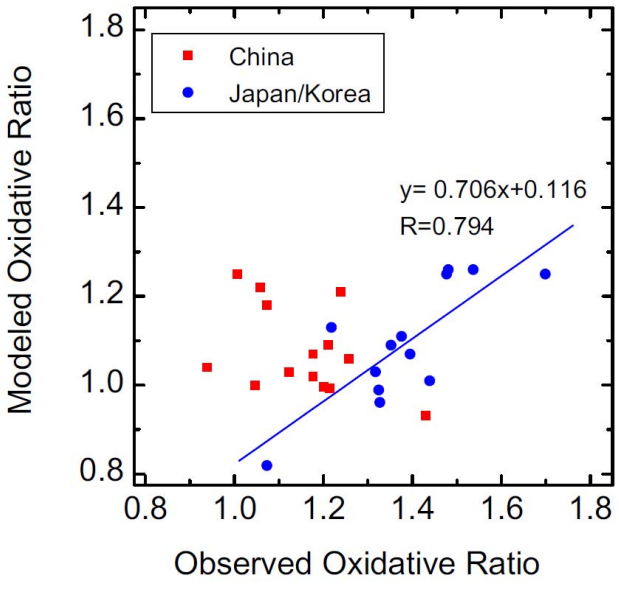

Fig. 7. Scatter plots of the oxidative ratios simulated by FLEXPART model simulation vs the observation for the pollution events from China and Japan/Korea. Red squares are the events from China and the blue circles are the events from Japan/Korea. The blue line represents a linear regression fit to the events from Japan/Korea.

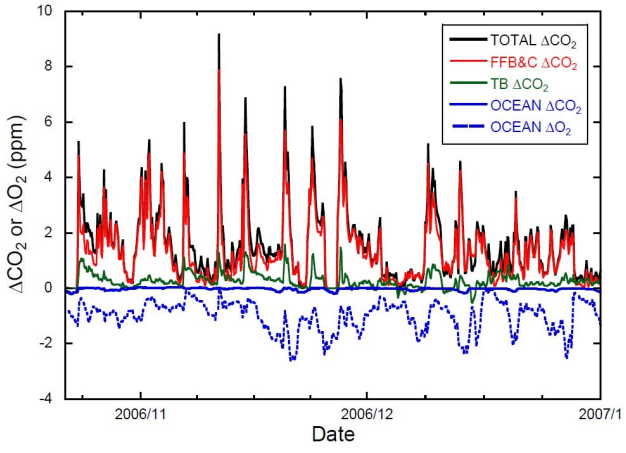

Fig. 8. Components of the ΔCO_2 variation at HAT calculated by FLEXPART. Black line is the total amount of CO_2 from the following three components, red line is the amount of $CO_2$from fossil fuel burning and cement production (FFBC), green line is from terrestrial bioshere (TB), and blue line is from the ocean. Oceanic ΔO_2 component is also plotted as broken blue line.

a result, the time series of the simulated oceanic O_2 component, shown in Fig. 8, sometimes show positive peak-like changes when the air masses are transported from the continental side. Such O_2 peaks could reduce the apparent magnitude of the O_2 depletion associated with the continental pollution events, resulting in the lower-than-biospheric oxidative ratios. Indeed, we find that removing the oceanic CO_2 and O_2 components in model simulations brings those averages closer to 1.10.

The simulated oxidative ratios by FLEXPART and the coupled model for the China events are very close to each other. Although the average values of the simulated oxidative ratios by FLEXPART and the coupled model for the Japan/Korea events show a small difference, but it is not significant with the 95 % confidence level from the Welch's t-test. These results suggest that the background influence to the oxidative ratios for the pollution events is relatively small.

4 Discussion

As described in the previous section, there are excellent agreements between the observed oxidative ratios and the calculated OR_{FFBC} based on the fossil fuel statistics for China and Japan/Korea. This result suggests that the synoptic-scale events at HAT are predominantly due to FFBC fluxes, and that the contributions from land biotic and oceanic fluxes are relatively small. To examine the contributions of individual flux components in short-term variations, the ΔCO_2 components derived from FFBC, TB and ocean are depicted in Fig. 8, which shows that most of the peaks come from FFBC emissions. This result can be explained by the fact that the distribution of the FFBC CO_2 emissions is localized in highly populated areas while that of the biospheric emissions is rather homogeneous. In addition, the localized FFBC CO_2 fluxes are generally one order and two orders of magnitude larger than the TB CO_2 and oceanic fluxes, respectively. (CO_2 is absorbed slightly by the ocean in the marginal region of East Asia at this time of the year.) The spatial distributions of the FFBC flux for 2006 and the TB and oceanic CO_2 fluxes for January are shown in Fig. 9. Thus, FFBC CO_2 appears as peaks while TB CO_2 is smeared as background.

In order to confirm that the emissions from FFBC are the main contributor to the simulated ORs and not the emissions from TB, two sensitivity tests were performed. First, a FLEXPART model simulation was performed in which the land biotic oxidative ratio was changed from 1.1 to 1.0, and the ORs for the pollution events were then recalculated. Second, the national OR_{FFBC} for China was changed from 1.11 to 1.00, and then the ORs for the pollution events were recalculated after the FLEXPART model simulation. The results of the sensitivity tests are summarized in Table 2. The former experiment decreased the average OR for the China events from 1.08 to 1.05, while the average OR for the Japan/Korea events stayed at 1.09. The latter experiment decreased the average OR for China and Japan/Korea from 1.08 to 0.98 and 1.09 to 1.06, respectively. These results confirm that the average OR for the China events is much more sensitive to the Chinese national OR_{FFBC} than to the land biotic oxidative ratio. On the other hand, the average predicted OR for

Table 2. Summary of the sensitivity tests for the FFBC and land biotic oxidative ratio in China.

	FLEXPART		
Air mass origin	Original Results	OR_{FFBC}=1.0	$OR^*_{TB} = 1.0$
China	1.08 ± 0.10 (14)	0.98 ± 0.09 (14)	1.05 ± 0.09 (14)
Japan/Korea	1.09 ± 0.14 (13)	1.06 ± 0.17 (13)	1.09 ± 0.14 (13)
Other	1.15 ± 0.16 (14)	1.18 ± 0.18 (14)	1.13 ± 0.16 (14)

* OR_{TB} refers to an oxidative ratio for land biotic processes.

Japan/Korea events is also affected by the national OR_{FFBC} of China while it is insensitive to the value of the land biotic exchange ratio. It is consistent with the rather low value of the predicted OR for Japan/Korea. It suggests that the contribution of emissions from China to the pollution events assigned as Japan/Korea is overestimated in the model simulations and about 50 % of FFBC CO_2 contribution on average comes from China.

Figure 10 shows the footprints as determined by the FLEXPART simulation for representative pollution events observed at HAT. Figure 10a, b, and c correspond to the periods of 04:00–22:00 (LT) on 3 March 2008, 02:00 on 6 November–09:00 on 7 November 2007, and 01:00 on 14 March–14:00 on 15 March, 2008, respectively. The footprint [g-C m^{-3}] is defined as a product of the ratio of particle number in a grid cell in a pre-determined mixed layer height to the total particle number [no units], the residence time [day], and the anthropogenic FFBC CO_2 flux [g-C m^{-2} day] divided by the pre-determined mixing layer height of 1000 m. Thus, those grid cells, which have large flux and particle numbers, have large contribution to the observed signal at HAT. In Fig. 10, the distributions of the dispersed particles are also shown as thin-black contours. In addition, the red curves in the figure show the backward trajectories for the individual pollution events. Based on the trajectory analysis, the pollution event shown in Fig. 10a is shown to originate in China, and is consistent with its footprint. Although the both pollution events shown in Figures 10b and 10c are assigned origins in Japan/Korea, the distribution patterns of the footprints are significantly different. The former footprint (Fig. 10b) covers mainly Japan and Korea while the latter footprint (Fig. 10c) shows that the emissions from China contribute about 80 % of the pollution event.

In the FLEXPART simulation, pollution events categorized by the back trajectory analysis as Japan/Korea in origin almost always contain substantial contribution of Chinese fluxes, therefore their simulated average $\Delta O_2/\Delta CO_2$ value is closer to that of China. One possibility is that particle spread in the simulation seems to be wider than that in reality. One solution for the problem would be to use higher spatially and temporally resolved meteorological fields. More spatially and temporally resolved fluxes might help to improve the agreement between the simulated and the observed individual events in this study.

5 Conclusions

We examined the correlation between changes in atmospheric O_2 and CO_2 mixing ratios for selected pollution events observed at HAT between October 2006 and December 2008. The oxidative ratios calculated from the regression slopes ($-\Delta O_2/\Delta CO_2$ molar ratios) for these pollution events showed large variability with a range of 1.0 to 1.7. Based on the 5-day back trajectories calculated with METEX, the origins of the pollution events were categorized into 3 regions: China, Japan/Korea and "other origins". We found that there was a significant difference in the average oxidative ratio between China (OR = 1.14 ± 0.12) and Japan/Korea (OR = 1.37 ± 0.15) origins. These values are comparable to the oxidative ratios, which are estimated from the national fossil fuel inventories for the corresponding countries. The results suggest that the atmospheric O_2 and CO_2 measurements combined with back trajectory analysis could be used to constrain the compositions of fuel types from regional emissions.

In order to examine how the regional FFBC emissions affect the oxidative ratios of the atmospheric pollution events observed at HAT, we simulated the observed atmospheric CO_2 and O_2 changes using the atmospheric transport model FLEXPART and the coupled model driven by O_2 and CO_2 fluxes from FFBC, TB, and the ocean. Analysis of the relative contributions of individual CO_2 fluxes to the atmospheric variations revealed that most of the peaks associated with the pollution events at HAT were indeed attributable to the FFBC CO_2 emissions. With the assigned fluxes, the transport models were able to reconstruct, with a good agreement with the observation, the average oxidative ratio of the pollution events assigned to China. Additional sensitivity analysis showed that the oxidative ratio of the pollution events originating in China reflects about 90 % of the change in OR_{FFBC} for China. These results suggest that the observed OR at HAT could be used to detect changes in the composition of fossil fuel types used in China in the future.

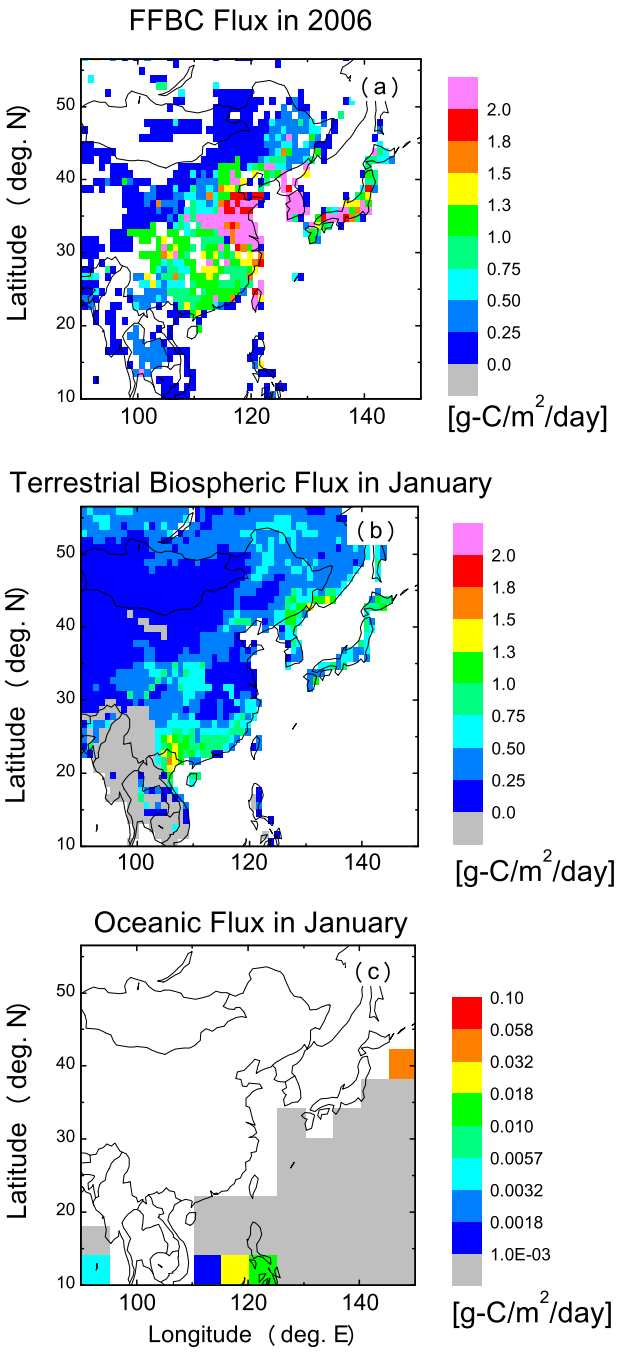

Fig. 9. The spatial distributions of **(a)** FFBC flux for 2006, **(b)** TB flux for January, and **(c)** oceanic CO_2 flux for January. These fluxes are used in the model simulation of this study.

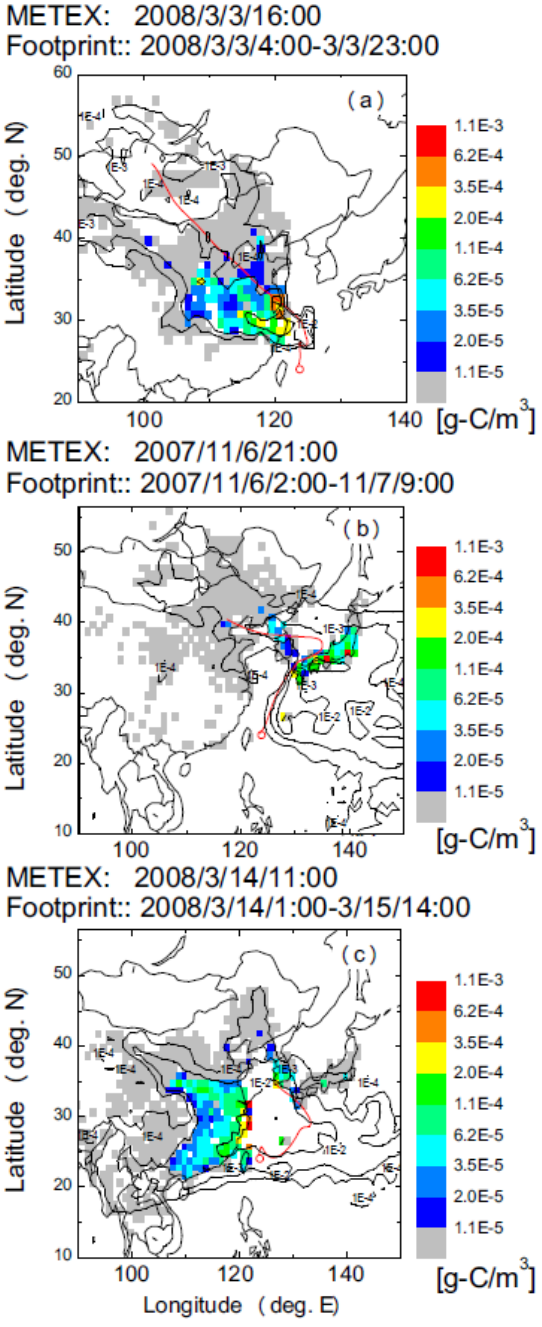

Fig. 10. Footprint for HAT calculated by FLEXPART for the cases in which air mass origins are assigned to **(a)** China, and **(b,c)** Japan/Korea by back trajectory analysis. **(b)** and **(c)** are the cases with small and large Chinese influence, respectively. Color scale is logarithmic. The distributions of the dispersed particles are also shown as thin-black contours, which represent the fraction of the number of particles that occur in each grid cell below the mixing layer height of 1000 m for the duration of backward simulation of 8 days. The red lines represent 5-day back trajectories calculated by METEX.

On the other hand, the model simulations underestimated the average OR for the Japan/Korea pollution events in comparison with the OR_{FFBC} for the Japan/Korea region. This is because the emissions from China make substantial contributions to the Japan/Korea pollution events in the model. This transport problem could be solved by using higher spatially

and temporally resolved meteorological fields in the model simulation than those used in this study, which has $1^\circ \times 1^\circ$ grid resolution. Using higher spatially resolved FFBC flux maps might also improve the agreement between the observed and simulated oxidative ratios for the Japan/Korea pollution events.

Acknowledgements. We are grateful to Nobukazu Oda of the Global Environmental Forum and local staffs for continuously supporting our in situ measurements. We also thank Toshinobu Machida and Kei-ichi Katsumata for determining CO_2 mixing ratios of the reference gases used at HAT and Shigeru Hashimoto for data processing of CO_2. We are grateful to Andreas Stohl for providing the FLEXPART model code. The datasets, JCDAS-25, used for this study are provided from the cooperative research project of the JRA-25 long-term reanalysis by the Japan Meteorological Agency (JMA) and the Central Research Institute of Electric Power Industry (CRIEPI). This work was financially supported by the Ministry of the Environment through the Global Environment Research Account for National Institutes (FY 2004–2008 (E0450), and FY2009-2010 (E0955)).

Edited by: M. Heimann

References

Boden, T. A., Marland, G., and Andres, R. J.: Global, Regional, and National Fossil-Fuel CO_2 Emissions, Carbon Dioxide Information Analysis Center, Oak Ridge National Laboratory, US Department of Energy, Oak Ridge, Tenn., USA, doi:10.3334/CDIAC/00001_V2010, available online: http://cdiac.ornl.gov/trends/emis/tre_glob.html, last access: 19 May 2011, 2010.

Garcia, H. E. and Keeling, R. F.: On the global oxygen anomaly and air-sea flux, J. Geophys. Res-Oceans., 106, 31155–31166, 2001.

Gregg, J. S., Andres, R. J., and Marland, G.: China: Emissions pattern of the world leader in CO_2 emissions from fossil fuel consumption and cement production, Geophys. Res. Lett., 35, L08806, doi:10.1029/2007GL032887, 2008.

Keeling, R. F.: Development of an interferometric oxygen analyzer for precise measurement of the atmospheric O_2 mole fraction, Ph.D., Harvard Univ., Cambridge, Mass., U.S.A., 178 pp., 1988.

Keeling, R. F. and Shertz, S. R.: Seasonal and interannual variations in atmospheric oxygen and implications for the global carbon cycle, Nature, 358, 723–727, 1992.

Kistler, R., Kalnay, E., Collins, W., Saha, S., White, G., Woollen, J., Chelliah, M., Ebisuzaki, W., Kanamitsu, M., Kousky, V., van den Dool, H., Jenne, R., and Fiorino, M.: The NCEP-NCAR 50-year reanalysis: Monthly means CD-ROM and documentation, B. Am. Meteorol. Soc., 82, 247–267, 2001.

Koyama, Y., Maksyutov, S., Mukai, H., Thoning, K., and Tans, P.: Simulation of variability in atmospheric carbon dioxide using a global coupled Enlerian-Lagrangian transport model, Geosci. Model Dev., 4, 317–324, doi:10.5194/gmd-4-317-2011, 2011.

Law, R. M., Peters, W., Rodenbeck, C., Aulagnier, C., Baker, I., Bergmann, D. J., Bousquet, P., Brandt, J., Bruhwiler, L., Cameron-Smith, P. J., Christensen, J. H., Delage, F., Denning, A. S., Fan, S., Geels, C., Houweling, S., Imasu, R., Karstens, U., Kawa, S. R., Kleist, J., Krol, M. C., Lin, S. J., Lokupitiya, R., Maki, T., Maksyutov, S., Niwa, Y., Onishi, R., Parazoo, N., Patra, P. K., Pieterse, G., Rivier, L., Satoh, M., Serrar, S., Taguchi, S., Takigawa, M., Vautard, R., Vermeulen, A. T., and Zhu, Z.: Transcom model simulations of hourly atmospheric CO_2: Experimental overview and diurnal cycle results for 2002, Global Biogeochem. Cy., 22, GB3009, doi:10.1029/2007gb003050, 2008.

Machida, T., Tohjima, Y., Katsumata, K., and Mukai, H.: A new CO_2 calibration scale based on gravimetric one-step dilution cylinders in National Institute for Environmental Studies-NIES 09 CO_2 scale, in: Report of the 15th WMO Meeting of Experts on Carbon Dioxide Concentration and Related Tracer Measurement Techniques, Jena, Germany, 7–10 September 2009, WMO/GAW Rep. 194, edited by: Brand, W., 114–118, WMO, Geneva, Switzerland, 2011.

Maksyutov, S., Patra, P. K., Onishi, R., Saeki, T., and Nakazawa, T.: NIES/FRCGC global atmospheric tracer transport model: description, validation, and surface sources and sinks inversion, J. Earth Sim., 9, 3–18, 2008.

Manning, A. C., Keeling, R. F., and Severinghaus, J. P.: Precise atmospheric oxygen measurements with a paramagnetic oxygen analyzer, Global Biogeochem. Cy., 13, 1107–1115, 1999.

Marland, G. and Rotty, R. M.: Carbon-dioxide emissions from fossil-fuels – a procedure for estimation and results for 1950–1982, Tellus B, 36, 232–261, 1984.

Marland, G., Boden, T. A., and Andres, R. J.: Global, regional, and national annual CO_2-emissions from fossil-fuel burning, cement production, and gas flaring: 1751–2002, NDP-030, Carbon Dioxide Inf. Anal. Cent., Oak Ridge Natl. Lab., http://cdiac.esd.ornl.gov/ndps/ndp030.html, last access: 19 May 2011, 2003.

Marland, G., Boden, T. A., and Andres, R. J.: Global, regional, and national CO_2 emissions, Carbon Dioxide Inf. Anal. Cent., Oak Ridge Natl. Lab., U.S. Dep. Of Energy, Oak Ridge, Tenn., http://cdiac.ornl.gov/trends/emis/tre/regn.html, last access: 3 August 2008, 2007.

Mukai, H., Katsumoto, M., Ide, R., Machida, T., Fujinuma, Y., Nojiri, Y., Inagaki, M., Oda, N., and Watai, T.: Characterization of atmospheric CO_2 observed at two-background air monitoring stations (Hateruma and Ochi-ishi) in Japan, Extended Abstract, Sixth International Carbon Dioxide Conference, 2–4 November 2011, I, 108–111, 2001.

Nakatsuka, Y. and Maksyutov, S.: Optimization of the seasonal cycles of simulated CO_2 flux by fitting simulated atmospheric CO_2 to observed vertical profiles, Biogeosciences Discuss., 6, 5933–5957, doi:10.5194/bgd-6-5933-2009, 2009.

Olivier, J. G. J. and Berdowski, J. J. M.: Global emissions sources and sinks, The Climate System, J. Berdowski, R. Guicherit, and B. J. Heij, A. A. Balkema Publishers/Swets and Zeitlinger Publishers, Lisse, The Netherlands, 33–78, 2001.

Seibert, P. and Frank, A.: Source-receptor matrix calculation with a Lagrangian particle dispersion model in backward mode, Atmos. Chem. Phys., 4, 51–63, doi:10.5194/acp-4-51-2004, 2004.

Severinghaus, J. P.: Studies of the Terrestrial O_2 and Carbon Cycles in Sand Dune Gases and in Biosphere 2, Ph.D., Columbia Univ., New York, NY, USA, 148 pp., 1995.

Shirai, T., Yokouchi, Y., Sugata, S., and Maksyutov, S.: HCFC-22 flux estimates over east asia by inverse modeling from hourly observations at hateruma monitoring station, J. Geophys. Res.-Atmos. 115, D15303, doi:10.1029/2009jd012858, 2010.

Stephens, B. B., Keeling, R. F., and Paplawsky, W. J.: Shipboard measurements of atmospheric oxygen using a vacuum-ultraviolet absorption technique, Tellus B, 55, 857–878, 2003.

Stephens, B. B., Bakwin, P. S., Tans, P. P., Teclaw, R. M., and Baumann, D. D.: Application of a differential fuel-cell analyzer for measuring atmospheric oxygen variations, J. Atmos. Ocean. Tech., 24, 82–94, 2007.

Stohl, A., Hittenberger, M., and Wotawa, G.: Validation of the Lagrangian particle dispersion model FLEXPART against large-scale tracer experiment data, Atmos. Environ., 32, 4245–4264, 1998.

Takahashi, T., Sutherland, S. C., Sweeney, C., Poisson, A., Metzl, N., Tilbrook, B., Bates, N., Wanninkhof, R., Feely, R. A., Sabine, C., Olafsson, J., and Nojiri, Y.: Global sea-air CO_2 flux based on climatological surface ocean pCO_2, and seasonal biological and temperature effects, Deep-Sea Res. Pt. II., 49, 1601–1622, 2002.

Thoning, K. W., Tans, P. P., and Komhyr, W. D.: Atmospheric Carbon-Dioxide at Mauna Loa Observatory 2. Analysis of the NOAA GMCC Data, 1974–1985, J. Geophys. Res.-Atmos., 94, 8549–8565, 1989.

Tohjima, Y.: Method for measuring changes in the atmospheric O_2/N_2 ratio by a gas chromatograph equipped with a thermal conductivity detector, J. Geophys. Res.-Atmos., 105, 14575–14584, 2000.

Tohjima, Y., Machida, T., Utiyama, M., Katsumoto, M., Fujinuma, Y., and Maksyutov, S.: Analysis and presentation of in situ atmospheric methane measurements from cape Ochi-ishi and Hateruma island, J. Geophys. Res.-Atmos., 107, 4148, doi:10.1029/2001jd001003, 2002.

Tohjima, Y., Mukai, H., Machida, T., and Nojiri, Y.: Gas-chromatographic measurements of the atmospheric oxygen/nitrogen ratio at Hateruma island and cape Ochi-ishi, Japan, Geophys. Res. Lett., 30, 1653, doi:10.1029/2003GL017282, 2003.

Tohjima, Y., Mukai, H., Nojiri, Y., Yamagishi, H., and Machida, T.: Atmospheric O_2/N_2 measurements at two Japanese sites: Estimation of global oceanic and land biotic carbon sinks and analysis of the variations in atmospheric potential oxygen (APO), Tellus B, 60, 213–225, 2008.

Tohjima, Y., Mukai, H., Hashimoto, S., and Patra, P. K.: Increasing synoptic scale variability in atmospheric CO_2 at Hateruma Island associated with increasing East-Asian emissions, Atmos. Chem. Phys., 10, 453–462, doi:10.5194/acp-10-453-2010, 2010.

van der Laan-Luijkx, I. T., Karstens, U., Steinbach, J., Gerbig, C., Sirignano, C., Neubert, R. E. M., van der Laan, S., and Meijer, H. A. J.: CO_2, $\delta O_2/N_2$ and APO: observations from the Lutjewad, Mace Head and F3 platform flask sampling network, Atmos. Chem. Phys., 10, 10691–10704, doi:10.5194/acp-10-10691-2010, 2010.

Yamagishi, H., Tohjima, Y., Mukai, H., and Sasaoka, K.: Detection of regional scale sea-to-air oxygen emission related to spring bloom near Japan by using in-situ measurements of the atmospheric oxygen/nitrogen ratio, Atmos. Chem. Phys., 8, 3325–3335, doi:10.5194/acp-8-3325-2008, 2008.

Yokouchi, Y., Taguchi, S., Saito, T., Tohjima, Y., Tanimoto, H., and Mukai, H.: High frequency measurements of HFCs at a remote site in east Asia and their implications for Chinese emissions, Geophys. Res. Lett., 33, L21814, doi:10.1029/2006gl026403, 2006.

Zeng, J. Y., Tohjima, Y., Fujinuma, Y., Mukai, H., and Katsumoto, M.: A study of trajectory quality using methane measurements from Hateruma island, Atmos. Environ., 37, 1911–1919, doi:10.1016/S1352-2310(03)00048-7, 2003.